RevMexAA (Serie de Conferencias), **37**, 120–131 (2009)

AGN AND STARBURST IN BRIGHT SEYFERT GALAXIES: FROM IR PHOTOMETRY TO IR SPECTROSCOPY

L. Spinoglio,[1] S. Tommasin,[1] and M. A. Malkan[2]

RESUMEN

La fotometría infrarroja y más recientemente la espectroscopía infrarroja proporcionan un diagnóstico poderoso para discriminar entre los principales mecanismos de emisión en galaxias AGN y Starbursts. A partir de la fotometría infrarroja pionera realizada por *IRAS* en el lejano-IR y el trabajo fundamental en San Pedro Mártir y en ESO en el cercano-IR, la fotometría de ISO logró extender hasta 200 μm la cobertura de las distribuciones de energía en galaxias. Ahora, *Spitzer* ha obtenido espectroscopía muy precisa en el mediano-IR en diversas muestras de galaxias. Revisaremos el trabajo realizado en la muestra de galaxias a 12 μm desde la época de la fotometría de *IRAS* hasta la nueva espectroscopía de *Spitzer*. Se presentan y discuten los principales resultados de los datos de multifrecuencia a 12 μm de las galaxias Seyfert seleccionadas a la luz de los modelos de unificación y evolución. El acervo espectroscópico de *Spitzer* será pronto extendido a longitudes de onda más largas con los espectrómetros en *Herschel* y en un futuro con *SPICA* a mayores corrimientos al rojo.

ABSTRACT

Infrared photometry and later infrared spectroscopy provided powerful diagnostics to distinguish between the main emission mechanisms in galaxies: AGN and Starburst. After the pioneering work on infrared photometry with *IRAS* in the far-IR and the San Pedro Martir and ESO ground-based work in the near-IR, ISO photometry extended up to 200 μm the coverage of the galaxies energy distributions. Then *Spitzer* collected accurate mid-infrared spectroscopy on different samples of galaxies. We will review the work done on the 12 μm galaxy sample since the times of *IRAS* photometry to the new *Spitzer* spectroscopy. The main results on the multifrequency data of 12 μm selected Seyfert galaxies are presented and discussed in the light of unification and evolution models. The spectroscopic work of *Spitzer* will soon be complemented at longer wavelengths by the *Herschel* spectrometers and in the future by *SPICA* at higher redshift.

Key Words: galaxies: active — galaxies: starbursts — infrared: galaxies

1. INTRODUCTION

The interrelationship between *star formation* and *accretion* onto massive black holes is crucial to understanding galaxy formation and evolution. On a cosmic scale, the evolution of supermassive black holes appears tied to the evolution of the star-formation rate (Marconi et al. 2004; Merloni et al. 2004). The growth of bulges through *star formation* may be directly linked to the growth of black holes through accretion (Heckman et al. 2004). On a local scale, evidence is mounting that *star formation* and nuclear activity are linked. Two possible evolutionary progressions can be predicted: HII/Starburst galaxies → Seyfert 2 (Storchi-Bergmann et al. 2001; Kauffmann et al. 2003), or a fuller scenario of HII/Starburst galaxies → Seyfert 2 → Seyfert 1 (Hunt & Malkan 1999; Levenson et al. 2001; Krongold et al. 2002). These predict that galaxy interactions, leading to the concentration of a large gas mass in the circumnuclear region of a galaxy, trigger starburst emission. Then mergers and bar-induced inflows can bring fuel to a central black hole, stimulating AGN activity. While relatively young ($\sim$ 1 Gyr) stellar populations are found in more than half of Seyfert 2s (Schmitt et al. 1999; González Delgado et al. 2001; Raimann et al. 2003), they are also found in broadlined AGNs (Kauffmann et al. 2003). However, any firm conclusion cannot rely on optical spectra of optically selected samples of galaxies. Photometric mid-IR studies (Edelson, Malkan, & Rieke 1987; Maiolino et al. 1995) did indeed find that Seyfert 2s galaxies more often have enhanced star formation than Seyfert 1s and the near and far-IR observations of the 12 μm galaxy sample (Spinoglio et al. 1995) show systematic differences between type 1's and type 2's spectral energy distributions. However, detailed *in-*

[1]Istituto di Fisica dello Spazio Interplanetario, INAF, Via Fosso del Cavaliere 100, I-00133, Roma, Italy (luigi.spinoglio, silvia.tommasin@ifsi-roma.inaf.it).

[2]Astronomy Division, University of California, Los Angeles, CA 90095-1547, USA (malkan@astro.ucla.edu).

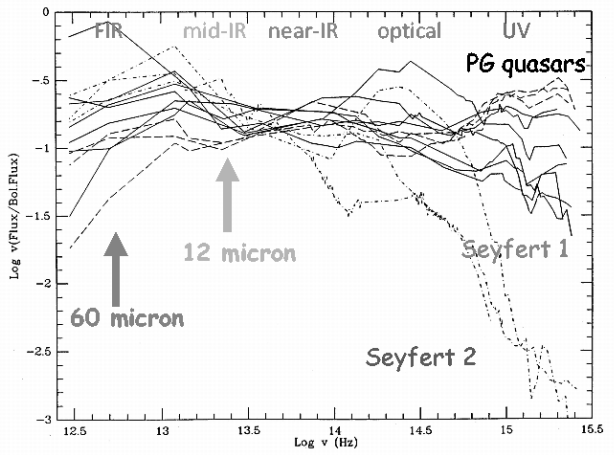

Fig. 1. Spectral energy distributions of 13 AGN normalized to the bolometric fluxes (Spinoglio & Malkan 1989).

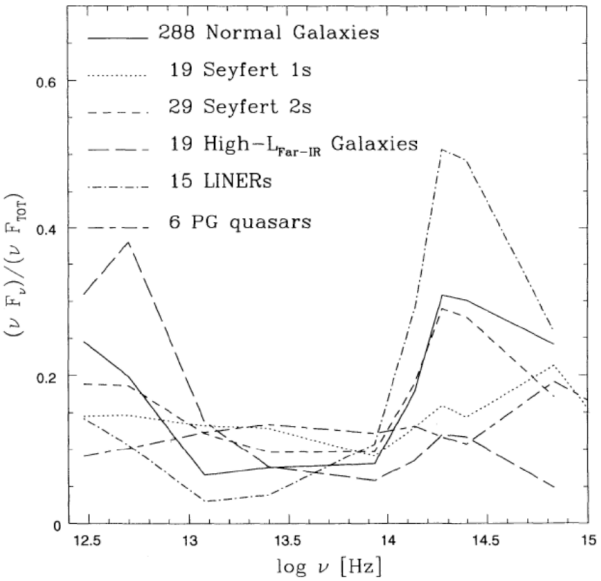

Fig. 2. Average SEDs of the various types of galaxies normalized to their bolometric fluxes (Spinoglio et al. 1995).

frared spectroscopy is necessary to better separate the star formation and accretion components in the energy budget of active galaxies and strengthen the hypothesis of an evolutionary difference between different types of active galaxies. Better understanding the *star formation* versus *accretion* connection requires mid-infrared spectroscopy of representative samples of active galaxies in the local universe. This is because active galactic nuclei (AGNs) are often very dusty, locally and even at high redshifts (Priddey et al. 2003; Bertoldi et al. 2003). Similarly, *star formation* activity, which often coexists with AGN activity, is also heavily enshrouded in dust.

We review in this article the great amount of observational work that has been done on the 12 μm galaxy sample and in particular on its subsample of active galaxies.

2. THE 12 μM ACTIVE GALAXIES SAMPLE

The sample that is less biased and most representative of the local active galaxies populations is selected from the 12 μm Galaxy Sample (12MGS), an IRAS-selected all-sky survey flux-limited to 0.22 Jy at 12 μm (Rush, Malkan, & Spinoglio 1993, hereafter RMS) and form the complete sub-samples of Seyfert 1s and Seyfert 2s of the entire 12MGS. This is essentially a bolometric flux-limited survey outside the galactic plane, because of the empirical fact that all *galaxies* emit a constant fraction of their total bolometric luminosity at 12 μm. This fraction is $\sim 9-13\%$ for AGNs and $\sim 7-8\%$ for normal and starburst galaxies, independent of star formation activity (Spinoglio et al. 1995). For Seyfert galaxies and quasars, this can be seen in Figure 1, which shows the spectral energy distributions of 13 active galaxies normalized to their bolometric flux: the minimum scatter among the different types of galaxies appears in the range 7–12 μm (Spinoglio & Malkan 1989). For the different types of 12 μm selected galaxies, normal, Seyfert, starburst galaxies and LINERs, compared to a small sample of PG quasars, the spectral energy distributions normalized to their bolometric fluxes are shown in Figure 2. Finally, the 12MGS is less subject to contamination by high star-formation rate objects than other infrared samples defined at longer wavelengths (Hunt & Malkan 1999).

12 μm selection finds obscured objects via reradiation of their primary emission by dust. An alternative way of finding obscured AGN is by selecting directly on their accretion radiation at hard X-rays, insensitive to all but the heaviest intrinsic absorption. However, unlike the 12MGS, as shows Figure 3, the hard X-ray selected samples miss most of the Compton thick objects ($N_{\rm H} > 10^{24}$ cm^{-2}).

The 12MGS contains 53 Seyfert 1s and 63 Seyfert 2s (RMS). This sample has a complete set of observations at virtually every wavelength: full IRAS and near-IR coverage (RMS; Spinoglio et al. 1995), X-rays (Rush et al. 1996), optical spectroscopy, radio (Rush, Malkan, & Edelson 1996), optical/IR imaging (Hunt & Malkan 1999; Hunt et al. 1999), 100–200 μm far-infrared photometry from ISOPHOT (Spinoglio, Andreani, & Malkan 2002). In the recent years 10 μm imaging (Gorjian et al. 2004),

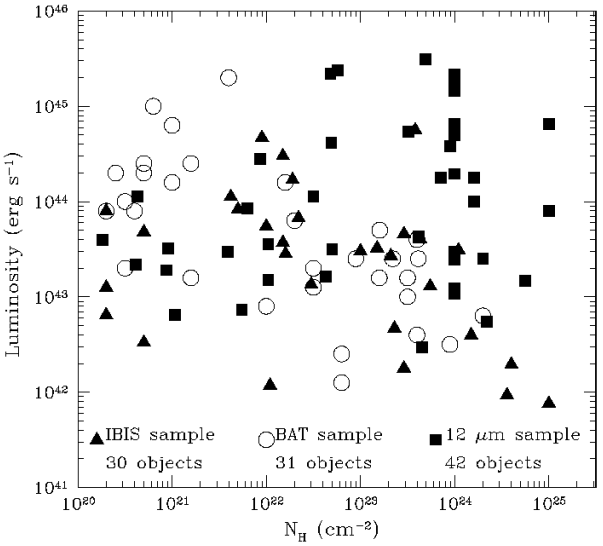

Fig. 3. Luminosity-Hydrogen absorption column density *plane* of the 12 μm Seyfert (squares) detected at hard X-rays. Hard-X-ray selected AGNs, from IBIS (triangles) and Bat (circles), are shown for comparison.

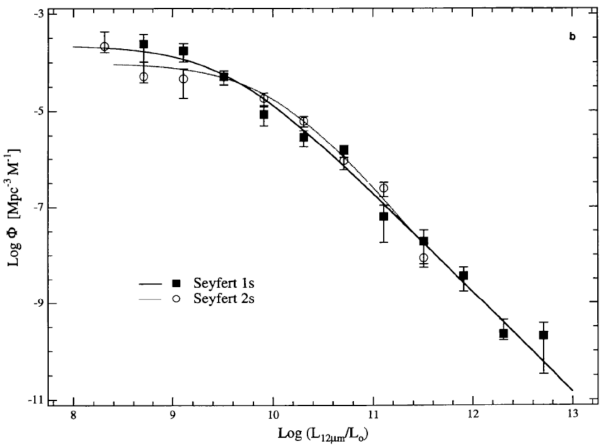

Fig. 4. The 12 μm luminosity function of Seyfert galaxies (RMS).

2.8–4.1 μm slit spectroscopy (Imanishi 2003; Imanishi & Alonso-Herrero 2004) optical spectropolarimetry (Tran 2001, 2003) radio observations (Thean et al. 2000, 2001) and *Spitzer* low resolution spectra (Buchanan et al. 2006) have been collected for most of the Seyfert galaxies in our sample. Finally a first article on the high resolution *Spitzer* spectra has been published (Tommasin et al. 2008) and another one is completing the mid-infrared spectral coverage of almost all the sample (Tommasin et al., in preparation).

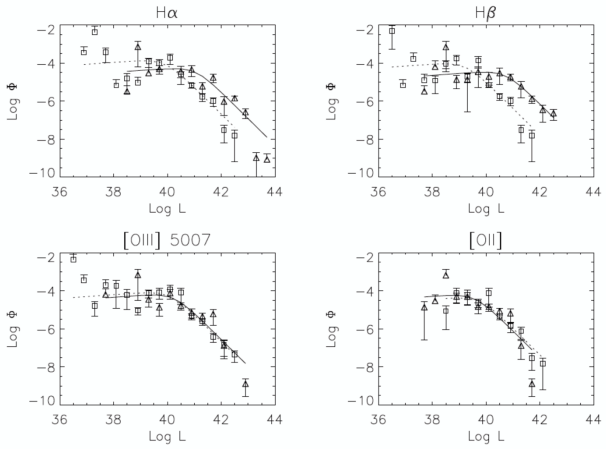

Fig. 5. Emission line luminosity functions for Hα, Hβ, [OIII]λ5007Å and [OII]λ3727Å for the 12 μm selected Seyfert galaxies (Rodriguez et al., in prep.). Triangles represent Seyfert 1's and squares Seyfert 2's.

2.1. *The 12 μm and the line luminosity functions of Seyfert galaxies*

The 12 μm luminosity function of the Seyfert galaxies of the 12MGS has been derived by RMS. There is no significant difference between the two types of Seyfert, as one can see from Figure 4, except for the fact that at the highest luminosities ($L > 10^{12}\ L_\odot$) only type 1's are found. We note, however, that this can be due to the inclusion in this latter class of the few blazars and quasars present in the 12MGS.

The analysis of the optical and ultraviolet emission line spectra has been done recently (Rodriguez et al., in preparation). The luminosity functions of all the narrow lines for which there is enough statistics ([OI]λ6300Å, [OII]λ3727Å, [OIII]λ4959Å, [OIII]λ5007Å, [NII]λ6584Å and [SII]$\lambda\lambda$6717+6734Å) are the same for both types of Seyfert's. Only the Hα and Hβ luminosity functions show more Seyfert 1's at high luminosities compared to Seyfert 2's. This difference can be understood because type 1's have substantial emission in both these lines from their Broad Line Regions. The luminosity functions for Hα, Hβ, [OIII]λ5007Å and [OII]λ3727Å are displayed in Figure 5.

The agreement between the 12 μm continuum and the narrow lines luminosity functions testifies that these quantities are all isotropic and are not affected by the geometry or disk/torus orientation. This also implies that the 12 μm selection is not biased against or in favor of Seyfert types 1 or types 2.

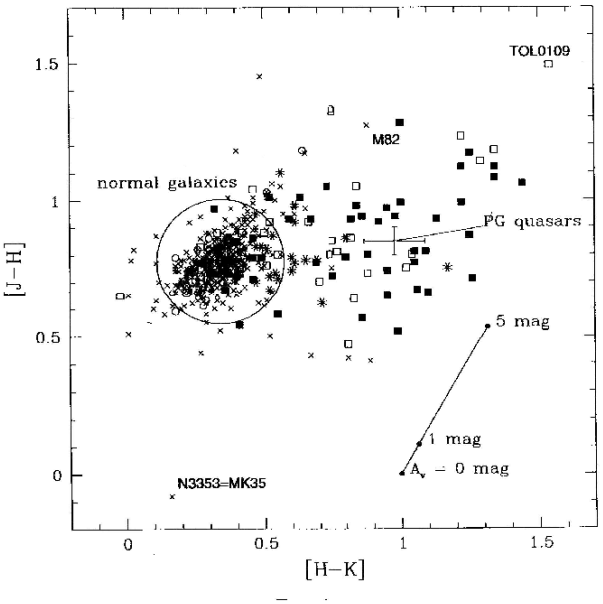

Fig. 6. [J-H] *vs* [H - L] diagram with Seyfert 1's (filled squares), Seyfert 2's (open squares), Normal's (crosses) (Spinoglio et al. 1995).

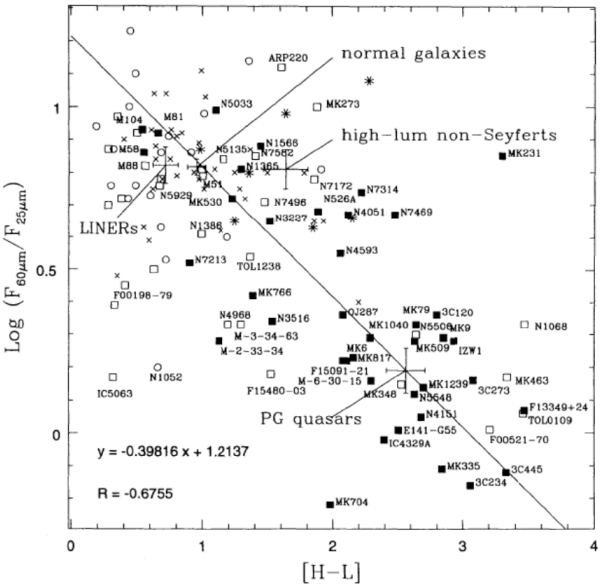

Fig. 7. Composite near-far-IR color-color diagram: the [H-L] color versus the 60 μm/25 μm flux ratio (Spinoglio et al. 1995).

3. INFRARED PHOTOMETRY

3.1. *Total near-infrared fluxes*

Infrared photometry has been used to isolate star formation and accretion processes. A large observational effort has been done to observe in the J, H, K and, in some cases, L bands as many as 321 galaxies from the 12 μm galaxy sample (Spinoglio et al. 1995). At the 2.1 m telescope of the S. Pedro Martir Observatory, thanks to a collaboration with Luis Carrasco and Elsa Recillas, we observed the northern galaxies, while those of the southern hemisphere were observed at the 1m ESO telescope (La Silla, Chile).

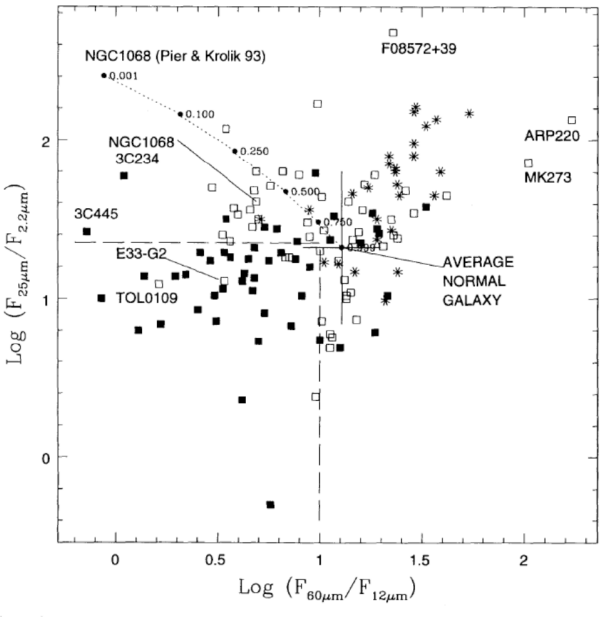

Fig. 8. Color-color diagram separating Seyfert 1's, 2's and starburst galaxies. The dotted line shows a mixture of the NGC 1068 torus model colors (Pier & Krolik 1993) and the average galactic colors. The symbols are the same as in the previous figure (Spinoglio et al. 1995).

To be able to compare the large beam IRAS data (RMS) with the near-IR data, derive spectral energy distributions and build meaningful color-color diagrams, we have computed the near-IR total fluxes using growth curves (Spinoglio et al. 1995). Combining the IRAS and near-IR data we were able to derive the spectral energy distributions (SED) of hundreds of galaxies. As presented in the previous section, we show in Figure 2 the average SEDs, normalized to their bolometric flux, of normal, Seyfert and starburst galaxies, as well as LINERs and PG quasars.

We have found that color-color diagrams are very effective in separating the different galaxy types. The usual [J-H] versus [H-K] color-color diagram shown in Figure 6 can separate many Seyfert galaxies from normal galaxies: at 2.2 μm the strong thermal emission from hot dust grains illuminated by the active nucleus rises above starlight from red giants, peaking in the H photometric band and dominating the stellar component in galaxies.

In Figure 7 we show the [H-L] color versus the 60 μm/25 μm flux ratio. This plot can separate normal and starburst galaxies from Seyfert type 1 and PG quasars, because the former have steep far-IR slopes and bluer near-IR spectra, while the latter have flatter far-IR SEDs and redder near-IR slopes. As most Seyfert 1's are located at the lower right part of the diagram, while most type 2's lie in the upper left corner, where only a few Seyfert 1's are found (most of which are nearby Messier galaxies) demonstrate that the SEDs of the two Seyfert populations are indeed different.

In Figure 8 we show the 60 μm/12 μm versus the 25 μm/2.2 μm, as suggested previously for an analysis of the CfA Seyfert galaxies (Edelson, Malkan, & Rieke 1987), where it is clear a segregation of the Seyfert type 1's in the lower left part of the diagram, at the flatter spectral slopes: 30/48 type 1s and only 5/52 type 2s occupy this region. The presence of an optically thick edge-on torus (Pier & Krolik 1993) would indeed steepen the SED by absorbing high energy radiation and re-emitting it at longer wavelengths.

3.2. *Bolometric luminosities of Seyfert and normal galaxies*

Spinoglio et al. (1995) determined for the first time the bolometric luminosities of a large sample of galaxies, both Seyfert and normal galaxies. One of their most important result is the linear relation found between the 12 μm and *bolometric* luminosities for both Seyfert and normal galaxies.

To obtain reliable *bolometric luminosities* for the galaxies, we have used the IRAS [60–100 μm] color to predict the far-IR turnover. Figure 9 shows the correlation between color temperature and IRAS spectral index. From the fit shown, we derived the relation:

$$T_{\rm color} = 11.4 \times (\alpha_{60-100\ \mu{\rm m}} + 4.67){\rm K}$$

We then computed the submillimeter fluxes beyond 100 μm assuming a graybody at the derived color temperature, with a dust emissivity $\epsilon \propto \lambda^{-1}$.

For the Seyfert galaxies, the relation between the 12 μm and the bolometric luminosity is shown in Figure 10, with a slope of 1.09 (with a regression coefficient of R=0.95). We notice that a similar relation between bolometric luminosity and the other IRAS bands monochromatic luminosities is poorer compared to the 12 μm band: at 25 μm the slope is 1.19 (R=0.90), at at 60 μm the slope is 1.19 (R=0.91) and at 100 μm the slope is 1.13 (with a poorer R=0.93).

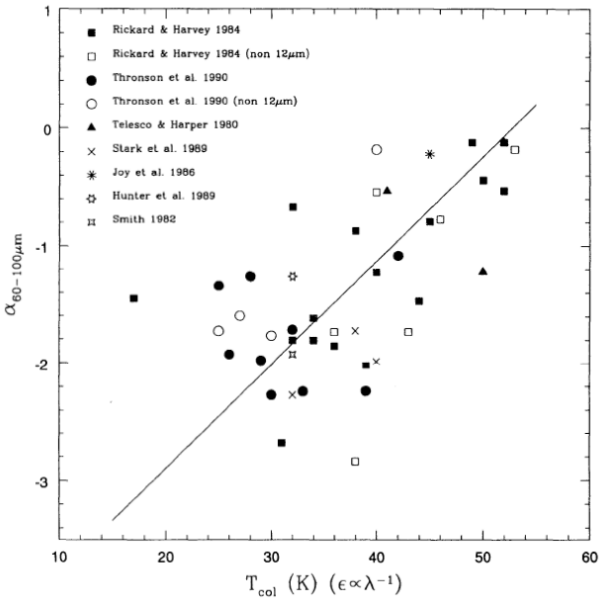

Fig. 9. Least squares fit of the spectral index $\alpha_{60-100\ \mu}$m as a function of the color temperature, assuming graybody emission (Spinoglio et al. 1995).

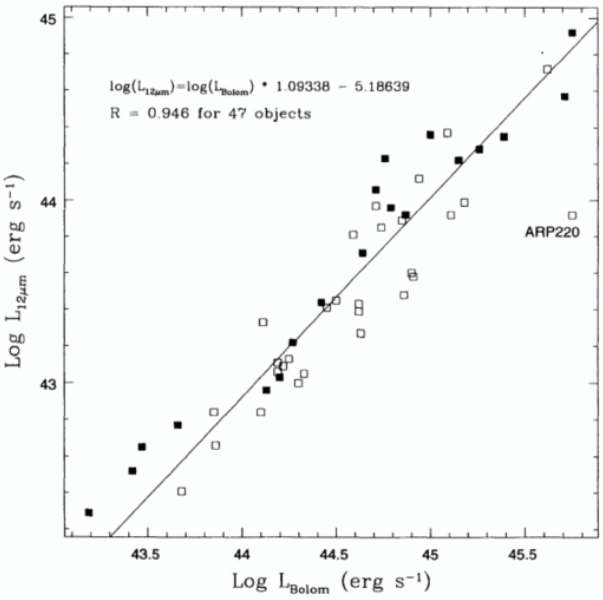

Fig. 10. 12 μm *vs* bolometric luminosity for Seyfert 1's (filled squares) and 2's (open squares). The line represents the least squares fit to all data, except Arp220 (Spinoglio et al. 1995).

For the normal galaxies, the relation between the 12 μm and the bolometric luminosity is shown in Figure 11, with a slope of 1.06 (with a regression coefficient of R=0.94). A similar relation between bolometric luminosity and the other IRAS bands

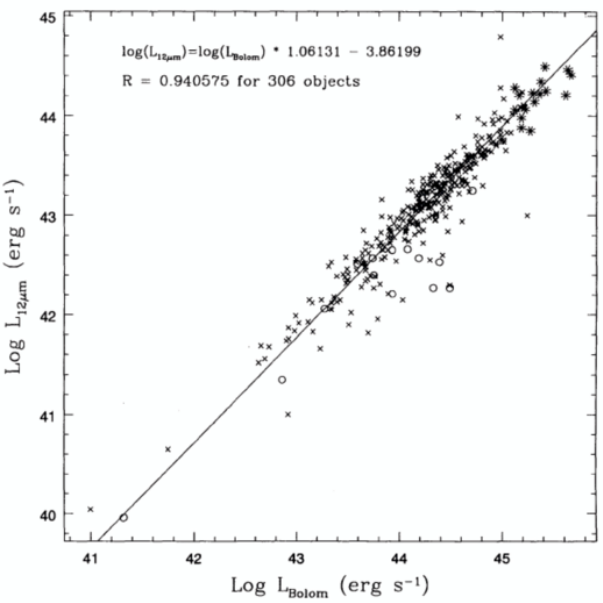

Fig. 11. 12 μm *vs* bolometric luminosity for normal galaxies (crosses), starburst's (asterisks) and LINERs (open circles). The line represents the least squares fit to all data (Spinoglio et al. 1995).

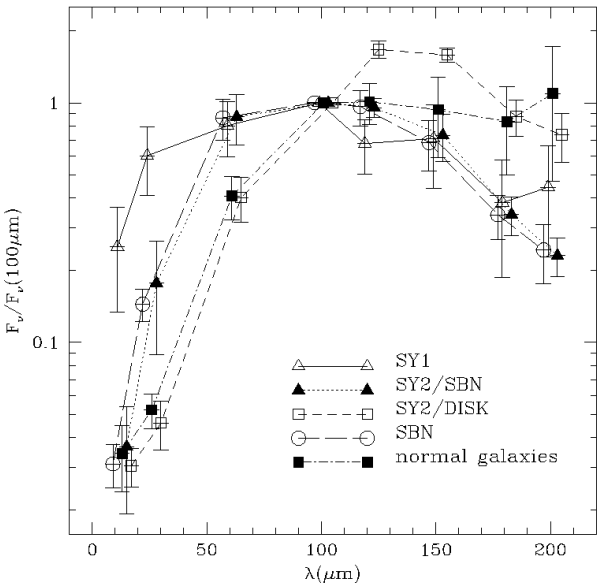

Fig. 12. The average spectral energy distributions of Seyfert, starburts and normal galaxies, normalized to the 100 μm flux (Spinoglio, Andreani, & Malkan 2002).

monochromatic luminosities is poorer compared to the 12 μm band: at 25 μm the slope is 1.15 (R=0.93), at at 60 μm the slope is 1.12 (R=0.94) and at 100 μm the slope is 1.11 (with a poorer R=0.89).

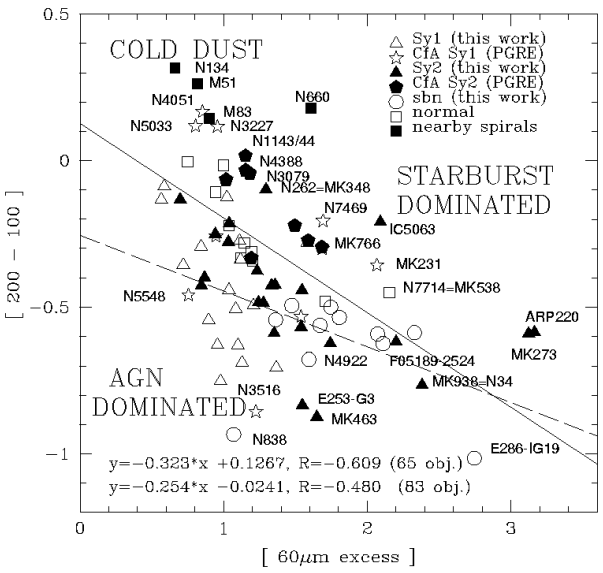

Fig. 13. [200–100 μm] color vs. the 60 μm excess diagram of galaxies belonging to the 12 μm galaxy sample (Spinoglio, Andreani, & Malkan 2002).

3.3. *Extending to 200 μm with ISO*

With the launch of the *Infrared Space Observatory*, we were able to collect far-infrared photometry between 100 and 200 μm for the 12 μm galaxies (Spinoglio, Andreani, & Malkan 2002). We have followed Rowan-Robinson & Crawford (1989) in using the 12–25–60–100 μm colors to identify those galaxies in our sample that closely resemble the SEDs of the *quiescent cirrus* disk, the starburst component, and the *pure Seyfert* nucleus. For each of the three types of galaxies –the normal spirals, the starburst galaxies, and the Seyfert 1's– we have selected those objects lying in the two IRAS color-color diagrams close (i.e., within 0.2 mag) to the colors of *pure disk*, *starburst*, and *Seyfert* components (Rowan-Robinson & Crawford 1989). We have plotted in Figure 12 the average 12–200 μm SEDs for each class. A strong distinction is apparent out to 200 μm between the quiescent disk component and the starburst component. These components represent the extremes of minimal and maximal recent star formation found in the least and most luminous galaxies, respectively. The pure Seyfert spectrum is rather similar to the pure starburst spectrum between 100 and 200 μm. Both show a relative lack of cold dust, and the Seyferts' spectra tend to be weaker at 120 μm.

The Seyfert 2's are spread all around the IRAS color-color diagrams. As can be seen in Figure 12, some of them (SY2/SBN) have IRAS spectra close to the pure starburst template. And indeed, their

ISOPHOT far-infrared spectra also match the pure starburst spectrum well, since their infrared continuum appears to be dominated from dust around star-forming regions. Those Seyfert 2's with IRAS colors like quiescent cirrus disks (SY2/DISK) also resemble pure disks in the 100–200 μm region. Again, it appears that the Seyfert 2 nucleus contributes a minor fraction of the observed far-infrared luminosity in those objects.

We have chosen as the indicator of enhanced recent star formation, which warms dust around HII regions, the 60 μm *excess* as the ratio of the observed 60 μm flux to the flux that a source would have at 60 μm from power-law interpolation of the flux between 12 and 100 μm (Figure 13).

While this diagram does not separate the galaxies of different classes perfectly, it nevertheless shows that they cluster preferentially in different regions of the diagram. Seyfert 1's (excluding six objects of the CfA sample) cluster in a 60 μm excess region with a color [200–100 μm] < 0. The starburst galaxies cluster in the central area of the diagram and have all 60 μm excess. Normal galaxies and nearby spirals have no 60 μm excess (except two objects) and a [200–100 μm] color between -0.5 and $+0.5$. Seyfert 2's are widely spread all over the diagram, but with a 60 μm excess generally higher than Seyfert 1's.

We suggest that the diagram shown in Figure 13 can be used to separate the starburst-dominated objects from the AGN-dominated ones. Objects located in the upper right part of the diagram are likely *starburst-dominated*, while those at the left, having a fainter excess, are the *AGN-dominated* objects. We suggest that starburst activity in galaxies, i.e., with high rates of current star formation, results in excess emission in the 60 μm band accompanied by a general heating of the galactic interstellar medium and thus a decrease of the [200–100 μm] color.

4. INFRARED SPECTROSCOPY

Mid-IR and far-IR spectroscopy of fine-structure emission lines are powerful tools to understand the physical conditions in galaxies.

Figure 14 shows the critical density (i.e. the density for which the rates of collisional and radiative de-excitation are equal) of a line versus the ionization potential of its ionic species. It shows how these lines can measure density and ionization of the gas: the ratio of lines with similar critical density, but different ionization potential, measures the ionization, while the ratio of lines with similar ionization potential, but different critical density, measures the density (Spinoglio & Malkan 1992). Lines from different emission regions in galaxies are shown with different symbols. Infrared spectroscopy has a thorough diagnostic power for gas with densities from 10^2 cm^{-3} to 10^8 cm^{-3} and ionization potentials up to 350 eV, using the so called coronal lines. Moreover, increasing its wavelength, an IR spectral line becomes more insensitive to dust extinction, and can therefore probe regions highly obscured at optical or even near-to-mid infrared wavelengths.

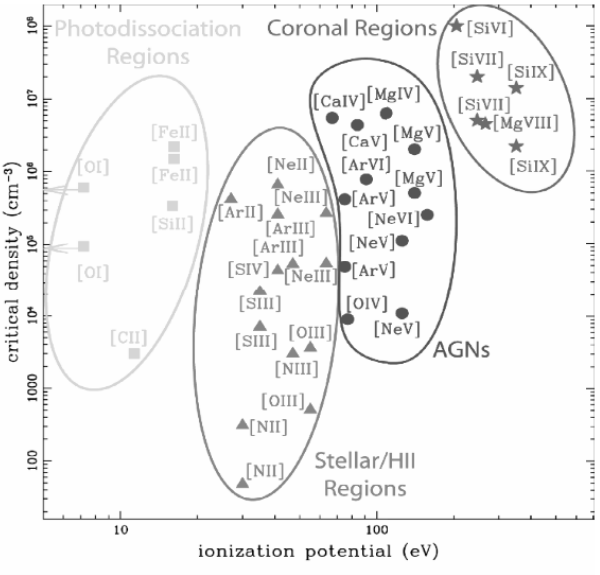

Fig. 14. The power of the infrared fine-structure lines to trace the different physical regimes. From left to right: low-ionization/photodissociation regions, stellar/HII regions, AGN emission line regions, Coronal line regions (Spinoglio & Malkan 1992).

Besides the ionic fine-sctructure lines, the mid-IR spectrum of galaxies also contains strong features due to the emission of Polycyclic Aromatic Hydrocarbons (Puget & Leger 1989), hereafter PAH. These features have been observed in ultraluminous IR galaxies with the *ISO* SWS spectrometer (Genzel et al. 1998). They are present while star formation is active and disappear when illuminated by the strong ionizing field of active nuclei.

4.1. *Far-IR spectroscopy with ISO-LWS*

Far-infrared spectroscopy has been so far collected by the LWS spectrometer onboard of *ISO* (Kessler et al. 1996) only on a few bright active and ultraluminous IR galaxies, showing an unexpected sequence of features from strong [OIII]52, 88 μm and [NIII]57 μm line emission to detection of only faint [CII]157 μm line emission and [OI]63 μm in absorption, and molecular lines almost always in absorption (Fischer et al. 1999). A few studies have been dedicated to individual galaxies, e.g. M82 (Colbert et al.

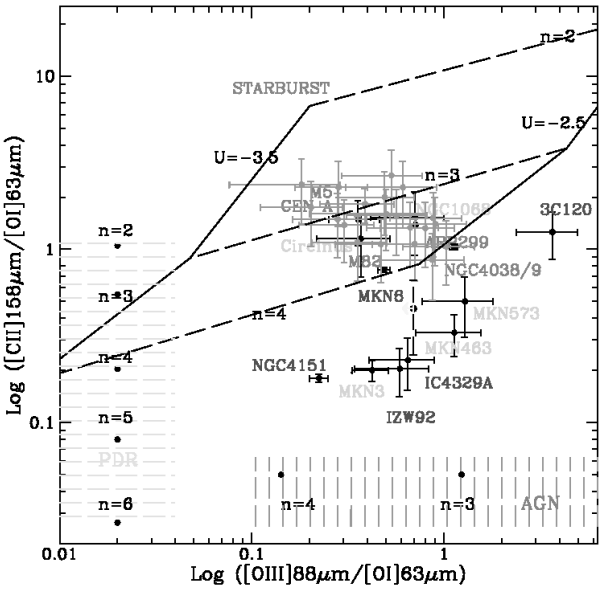

Fig. 15. ISO-LWS line ratio diagram (Spinoglio et al. 2003). Seyfert 1's: black symbols, starburst galaxies: grey symbols. Grey crosses: nearby galaxies (Negishi et al. 2001). Grid: starburst models with different densities and ionization parameter. Vertical dots on the left: the [CII]/[OI] ratio for PDR models for different densities (log n=2–6 cm^{-3}, log G_0=3). Horizontal dots at the bottom right: the [OIII]/[OI] ratio for AGN models (log U=−2.5, log n=3, 4 cm^{-3}).

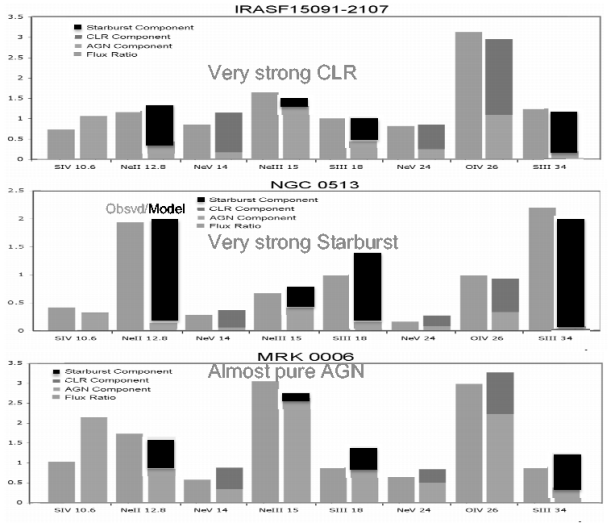

Fig. 16. Comparison of the observed and modelled spectra for three sample Seyfert galaxies (Hainline et al., in preparation).

1999), Arp220 (González-Alfonso et al. 2004), NGC 1068 (Spinoglio et al. 2005), Mrk231 (González-Alfonso et al. 2008). A systematic far-infrared spectroscopic survey of Seyfert and ULIRGs will have to wait for the *Herschel* mission. However the few data available already revealed the diagnostic power of the FIR fine structure lines. Figure 15 (Spinoglio et al. 2003) shows the [CII]158 μm/[OI]63 μm ratio versus the [OIII]88 μm/[OI]63 μm ratio. Normal galaxies cluster together with the Seyfert's having strong starburst emission (e.g. NGC 1068) and coincide with predicted ratios for typical starburst galaxies. However, at lower values of the [CII]/[OI] ratio, most of the AGN are clustering in a strip with higher ratio of [OI]/[CII] compared to starburst galaxies. This may arise from X-Ray Dissociation Regions (XDRs), whose [OI]/[CII] ratios are larger than in PDRs. Thus the 3 strongest FIR emission lines can separate the 3 basic energy sources in galaxies: (a) the AGN produces strongly emission from highly ionized gas, with [OIII] being a prominent in the NLR, but also unusually strong [OI]63 μm because this neutral line is strong in XDRs (Meijerink et al. 2007), and has a very high critical density ($\sim 10^6$ cm^{-3}). All the classical Seyfert galaxies in Figure 15 lie in the bottom part of the diagram, below any of the starburst models. (b) recent star formation, which produces [OIII] in the high-excitation HII regions, as well as strong [CII]158 μm in the PDRs which tend to surround these star forming regions; and (c) pure PDR emission from the quiescent disk of the spiral galaxy, which produces strong [CII] and [OI] emission, but no [OIII]. The most quiescent spirals lie in the upper left side of the diagram.

4.2. *Mid-IR spectroscopy with Spitzer*

In the very rich mid-infrared spectra of active galaxies we can identify various indicators of *AGN dominance*, e.g. the line ratios of [NeV]/[NeII], [NeV]/[SiII], [OIV]/[NeII], as well as indicators of *star formation dominance*, e.g. the PAH emission bands, the H_2 rotational lines and nebular emission lines mainly originated in HII regions, e.g. from [SIII] and [NeII].

The diagnostic power of the mid-IR fine structure lines can be quantified from the decomposition of the observed spectra in terms of three different components (Hainline et al., in prep.): (a) *AGN model*: with meteallicity Z solar, spectral slope $\alpha = -1.7$, density n=10^3, and ionization potential: log $U = -2$ (Groves et al. 2004); (b) *Starburst model*: with metallicity $Z = 2 \times Z_\odot$, age range = $0.1 - 6$ Myr, log $R = (\mathrm{Mcl}/M_\odot)/(\mathrm{Po}/k) = -6$, (Dopita et al. 2006); (c) *a Coronal line region model* (CLR): log $U = 0$ at the inner radius of the region and spectral slope $\alpha = -1.0$ (Spinoglio &

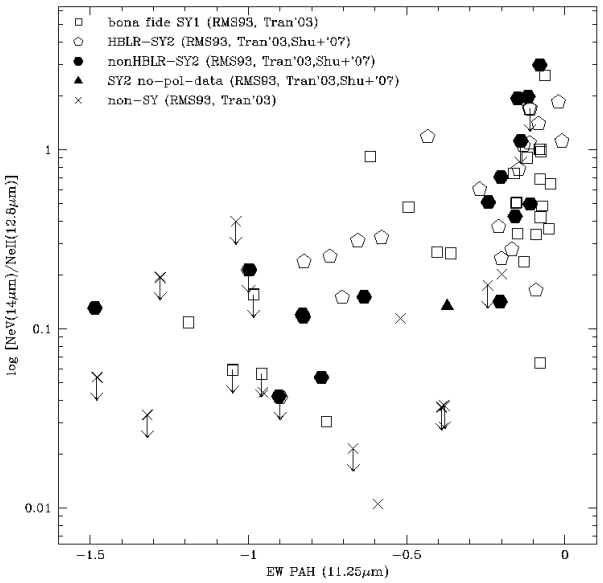

Fig. 17. [NeV]14.3 μm/[NeII]12.8 μm line ratio versus the equivalent width of the 11.25 μm PAH. (Tommasin et al. 2008; Tommasin et al., in prep.).

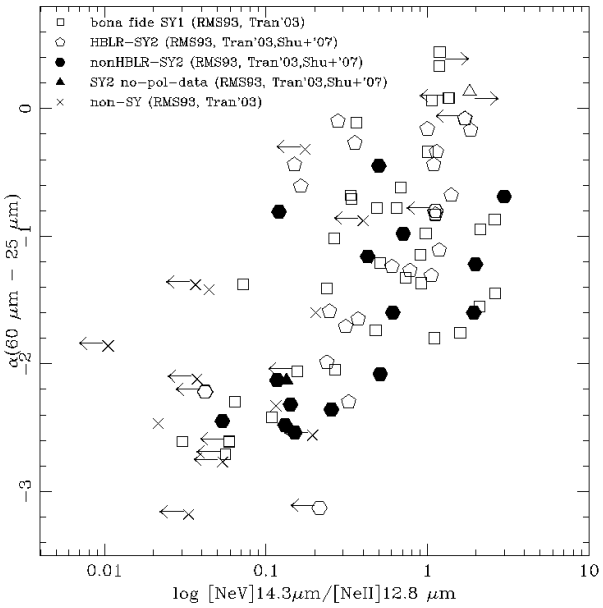

Fig. 18. The mid-to-far-IR spectral index $\alpha_{(60\ \mu m-25\ \mu m)}$ versus the [NeV]14.3 μm/[NeII]12.8 μm line ratio (Tommasin et al. 2008).

Malkan 1992). Figure 16 shows such a decomposition for the mid-IR spectra of three sample objects: IRASF15091-2107 for which a strong CLR is present, NGC 513 for which a strong Starburst component is necessary to fit the data and Mrk6, which is almost a "pure" AGN.

The first results of the *Spitzer* spectroscopic survey of the Seyfert galaxies of the 12 μm sample (Tommasin et al. 2008) show a clear inverse trend between the indicator of *AGN dominance* [NeV]14.3 μm/[NeII]12.8 μm line ratio and the equivalent width of the 11.25 μm PAH feature, which can be considered as an indicator of the *star formation dominance*, as shown in Figure 17. Here the Seyfert galaxies have been reclassified, following the results of spectropolarimetry Tran (2001, 2003), in type 1's (including the classical Seyfert 1's and the hidden Broad Line Region Seyfert 2's, as discovered through spectropolarimetry) and "pure" type 2's (for which a BLR was not detected). Most of the type 1 objects, including both Seyfert 1s and hidden Broad Line Region Seyfert 2s, are located at high values of the [NeV]14.3 μm/[NeII]12.8 μm line ratio and very low or absent PAH emission.

Another diagnostic diagram using both spectroscopic and photometric results is shown in Figure 18: the spectral index between 25 and 60 μm $\alpha_{(60\ \mu m-25\ \mu m)}$ versus the [NeV]14.3 μm/[NeII]12.8 μm line ratio. A clear trend shows that when the *AGN dominance* increases, the spectral index flattens. Most of type 1 objects appear to be concentrated in the upper right part of the diagram, at high values of *AGN dominance* and flat mid-to-far-IR slopes.

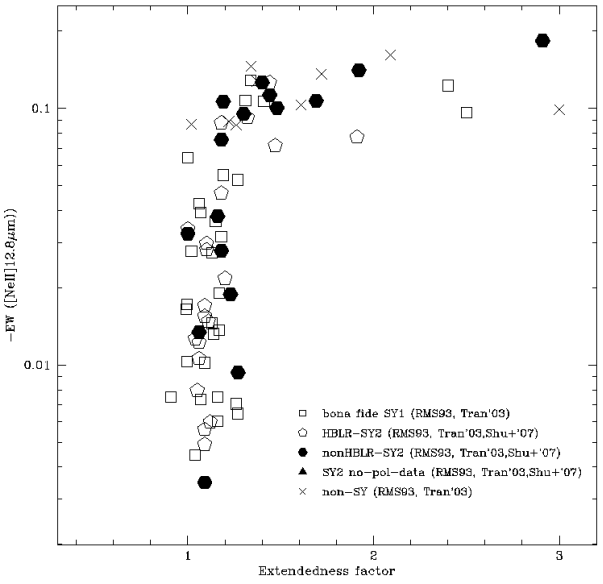

Fig. 19. [NeII]12.8 μm line equivalent width as a function of the source extendedness (Tommasin et al. 2008).

The two channels of the Spitzer high-resolution spectrometer: SH 9.6–19.5 μm with slit size 4.7″ × 11.3″ and LH 19–39 μm with slit size 11.1″×22.3″ al-

low "multi-aperture photometry" in the overlapping parts (19.0–19.5 μm). The ratio of the flux measured in LH to that measured in SH gives the "extendedness" of the source. We used this measure of the extendedness of the source to estimate the line emitting regions (Tommasin et al. 2008). In Figure 19 we plot the [NeII]12.8 μm line equivalent width as a function of the source extendedness. We notice that those sources showing a significant mid-IR extendedness are type 2 objects or non-Seyfert galaxies and have the highest [NeII]12.8 μm line equivalent width. An high [NeII]12.8 μm line equivalent width is a measure of a strong star formation component. This is not the case for the high excitation lines, originated from the AGN, such as [NeV] and [OIV], for which no apparent trent appears between source extendedness and line EWs (Tommasin et al. 2008).

5. ANALYSIS OF THE 12 μM SAMPLE MULTI-FREQUENCY DATASET

The 12MGS has been observed extensively from the radio to the X-rays and we can use the large set of data to search for correlations between different observed quantities. To show an example, we want to relate the X-ray luminosity, measuring the accretion, to the bolometric luminosity, as given by the 12 μm luminosity. We plot in Figure 20 the *unabsorbed* 2–10 keV luminosity and the 12 μm luminosity.

Following the finding of Spinoglio & Malkan (1989) and Spinoglio et al. (1995) that the 12 μm luminosity is linearly proportional to the *bolometric* luminosity, at a given L_{bol} in Figure 20 a sequence can be identified with decreasing accretion luminosity: from Seyfert 1's → HBLR-Seyfert 2's → *pure* Seyfert 2's. Although these results are to be considered preliminary, as no statistical method has yet been applied, most Seyfert 1's have: $0.1 \times L(12\ \mu\text{m}) < L(2-10\ \text{keV}) < L(12\ \mu\text{m})$ Most HBLR-Seyfert 2's have: $0.01 \times L(12\ \mu\text{m}) < L(2-10\ \text{keV}) < 0.1 \times L(12\ \mu\text{m})$ Most pure Seyfert 2's and non-Seyfert's have: $L(2-10\ \text{keV}) < 0.01 \times L(12\ \mu\text{m})$

We preminilarily suggest that black hole accretion, as measured by X-rays, is the dominant mechanism determining the observational nature of a galaxy: when accretion is not an important energy source, we have galaxies without Seyfert nuclei, dominated by stellar evolution processes (called here non-Seyfert's), then when accretion increases we have a sequence from the *pure* Seyfert 2's, to the HBLR-Seyfert 2's and finally when accretion dominates the bolometric luminosity, we have the Seyfert 1's.

In an analogous way, we try to correlate the IRAS 60 μm luminosity (measuring the integrated star formation activity) and the H_2 S(1) line luminosity (typical star formation indicator) in Figure 21.

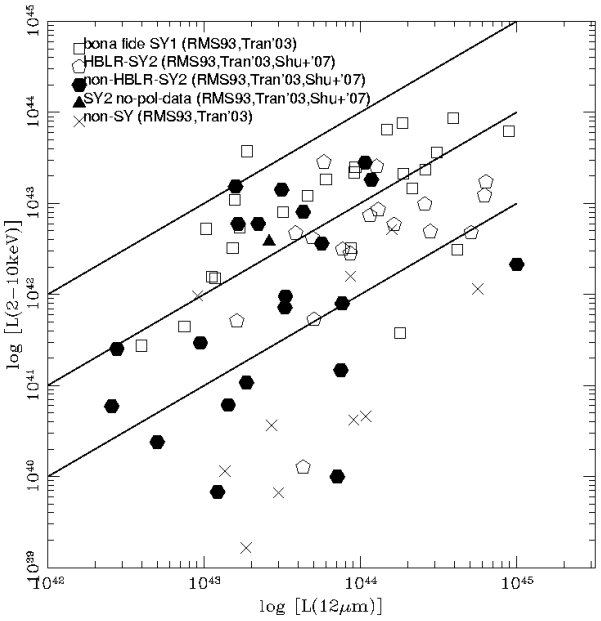

Fig. 20. Corrected (unabsorbed) X-ray (2–10 keV) luminosity as a function of the 12 μm luminosity. The three lines from the top to the bottom indicate the loci of L(2–10 keV) = L(12 μm) (top); L(2–10 keV) = 0.1 × L(12 μm) (middle); and L(2–10 keV) = 0.01 × L(12 μm) (bottom), which are used in the text to roughly separate the different objects.

Most Seyfert 1's and HBLR-Seyfert 2's have: $L(H_2) \sim 5 \times 10^{-4} \times L(60\ \mu\text{m})$ Most pure Seyfert 2's and non-Seyfert have: $L(H_2) \sim 10^{-4} \times L(60\ \mu\text{m})$

If we make least squares fits to the two extreme populations of Seyfert type 1's and non-Seyfert galaxies, we obtain a sequence of two almost parallel lines of the form $\log(L(60\ \mu\text{m})) = a \times \log(L(H_2)) + b$ from the bottom to the top:

- for Seyfert 1's: $a = 0.905$, $b = 7.325$, with a regression coefficient of R=0.928;
- for non-Seyfert's: $a = 1.030$, $b = 2.797$, with R=0.925.

There are two interpretations of this behavior: either the more active galaxies (type 1's) have enhanced H_2 emission (Rigopoulou et al. 2002), or at a given H_2 luminosity, type 2's (and non-Sy) have $L(60\mu m)$ 5 times higher than type 1's, because of an enhanced star formation process.

6. SPECTROSCOPY OF HIGHER REDSHIFT GALAXIES WITH HERSCHEL & SPICA

To understand how the two processes of black hole accretion and star formation shared the energy

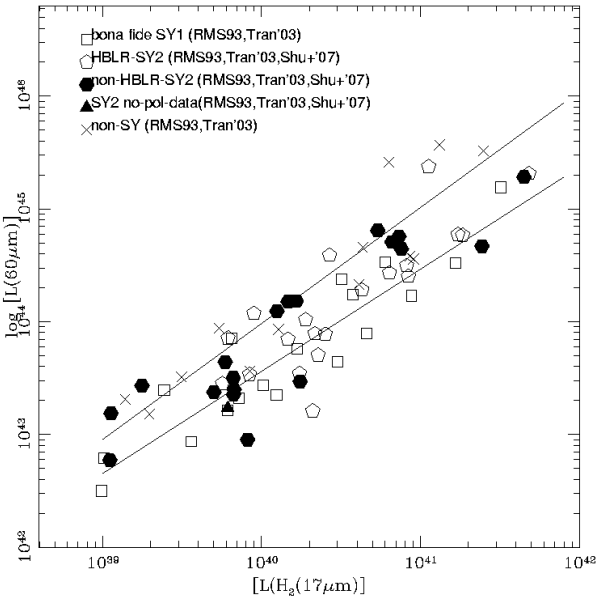

Fig. 21. Total 60 μm luminosity as a function of the H_2 17 μm line luminosity. The two lines from the top to the bottom least squares fits of the non-Seyfert galaxies and of the Seyfert 1's, respectively (see the text).

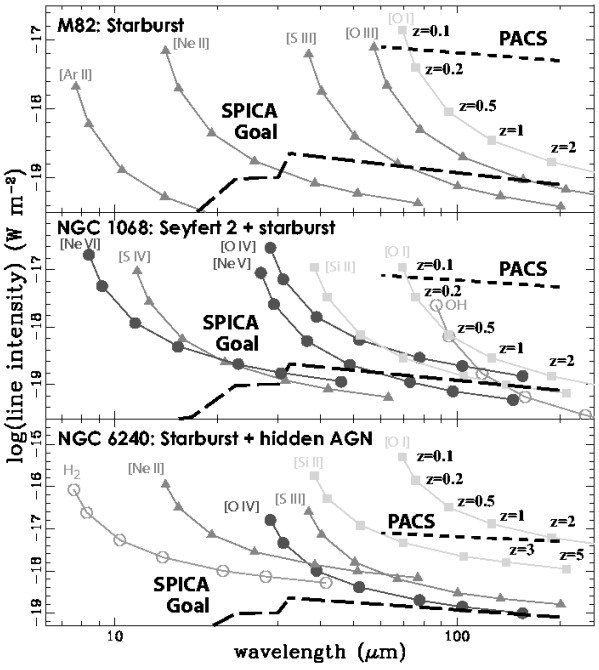

Fig. 22. Line observability with PACS onboard of *Herschel* and with *SPICA*. Few selected diagnostic lines are shown as a function of redshift for the three template objects M82, NGC 1068 and NGC 6240 (from the top to the bottom). The lines have the same symbols as in Figure 14, except for the open circles, representing molecular lines. Line intensities are given in W m^{-2}. The short dashed and long-dashed lines give the 5σ, 1 hour sensitivities of the PACS and SPICA spectrometers.

budget during galaxy evolution, we need to separate these two processes along the history of galaxies, and –to do this– rest-frame near-to-mid infrared spectroscopy is needed on galaxies as a function of their redshift. We predicted the line intensities of Seyfert and starburst galaxies at increasing redshift, considering the ISO spectra of three local template objects: NGC 1068 (Alexander et al. 2000; Spinoglio et al. 2005), the prototypical Seyfert 2 galaxy, containing both an AGN and a starburst; NGC 6240 (Lutz et al. 2003), a bright starburst with obscured AGN and M82 (Forster Schreiber et al. 2001; Colbert et al. 1999), the prototypical starburst galaxy. We then computed the line intensities as a function of redshift (in the range z=0.1–5), assuming that the line luminosities scale as the bolometric luminosity and that there is a luminosity evolution proportional to the $(z+1)^2$, consistent with the Spitzer results at least up to redshift z=2 (Perez-Gonzalez et al. 2005).

For simplicity[3], we adopted an Einstein-De Sitter model Universe, with $\Omega_\Lambda = \Omega_{\rm vac} = 0$ and $\Omega_M = 1$, $H_0 = 75$ km s^{-1} Mpc^{-1}. The luminosity distances have been derived using:

$$d_L(z) = (2c/H_0) \cdot [1 + z - (1+z)^{1/2}] .$$

The results for the three template objects are reported in a graphical form in Figure 22, where the intensities of selected lines are plotted as a function of the redshift. Among the brightest lines are shown the [SIV]10.5 μm, the [NeII]12.8 μm and the [OIII]52 μm diagnostic for the stellar/HII regions; the [NeV]24.3 μm and the [OIV]25.9 μm, for the AGN component, the [OI]63 μm and the [SiII]33.5 μm, for the photodissociation regions and the OH and H_2 rotational lines for the warm molecular component.

The 5σ, 1 hour sensitivities of the PACS spectrometer onboard of *Herschel* and of the two spectrometers foreseen at the focal plane of the JAXA mission *SPICA* (Space Infrared Telescope for Cosmology and Astrophysics) (Nakagawa 2004; Swinyard et al. 2008) are shown in the figure for comparison.

[3]We note that the dependence on different cosmological models is not very strong. The popular model with $\Omega_M = 0.27$, $\Omega_{\rm vac}=0.73$, $H_0=71$ km s^{-1} Mpc^{-1} shows greater dilutions, increasing with z, by factors of 1.5 for z=0.5 to 2.5 for z=5. In this case the line intensities of Figure 22 would decrease by these factors.

It is clear from the figure that the PACS spectrometer will be able to observe only the most favorable object (NGC6240) up to z=2 in the brightest line ([OI]63 μm), while the SPICA spectrometers *goal* sensitivities will allow deep infrared spectroscopic studies for all templates at z $\sim$ 1-2 for most lines and at z even higher for the brightest lines.

This work has been funded in Italy by the Italian Space Agency (ASI).

REFERENCES

Alexander, T., et al. 2000, ApJ, 536, 710
Bertoldi, F., et al. 2003, A&A, 406, L55
Buchanan, C., et al. 2006, AJ, 132, 401
Colbert, J. W., et al. 1999, ApJ, 511, 721
Dopita, M. A., et al. 2006, ApJS, 167, 177
Edelson, R. A., Malkan, M. A., & Rieke, G. H. 1987, ApJ, 321, 233
Fischer, J., et al. 1999, Ap&SS, 266, 91
Forster Schreiber, N. M., et al. 2001, ApJ, 552, 544
Genzel, R., et al. 1998, ApJ, 498, 579
González-Alfonso, E., et al. 2004, ApJ, 613, 247
_____. 2008, ApJ, 675, 303
González Delgado, R., Heckman, T., & Leitherer, C. 2001, ApJ, 546, 845
Gorjian, V., et al. 2004, ApJ, 605, 156
Groves, B. A., Dopita, M. A., & Sutherland, R. 2004, ApJS, 153, 9
Heckman, T. M., et al. 2004, ApJ, 613, 109
Hunt, L. K., & Malkan, M. A. 1999, ApJ, 516, 660
Hunt, L. K., et al. 1999, ApJ, 510, 637
Kauffmann, G., et al. 2003, MNRAS, 346, 1055
Kessler, M., et al. 1996, A&A, 315, L27
Krongold, Y., Dultzin-Hacyan, D., & Marziani, P. 2002, ApJ, 572, 169
Lutz, D., et al 2003, A&A,409, 867
Imanishi, M. 2003, ApJ, 599, 918
Imanishi, M., & Alonso-Herrero, A. 2004, ApJ, 614, 122
Levenson, N. A., Weaver, K. A., & Heckman, T. M. 2001, ApJ, 550, 230
Maiolino, R., Ruiz, M., Rieke, G. H., & Keller, L. D. 1995, ApJ, 466, 561
Marconi, A., et al. 2004, MNRAS, 351, 169
Meijerink, R., et al. 2007, A&A, 461, 793
Merloni, A., Rudnick, G., & Di Matteo, T. 2004, MNRAS, 354, 37
Nakagawa, T. 2004, Adv. Space Res., 34, 645
Negishi, T., et al. 2001, A&A, 375, 566
Perez-Gonzalez, P. G., et al. 2005, ApJ, 630, 82
Pier, E. A., & Krolik, J. H. 1993, ApJ, 418, 673
Priddey, R. S., Isaak, K. G., McMahon, R. G., Robson, E. I., & Pearson, C. P. 2003, MNRAS, 344, L74
Puget, J.-L., & Leger, A. 1989, ARA&A, 27, 161
Raimann, D., Storchi-Bergmann, T., González Delgado, R. M., Cid Fernandes, R., Heckman, T., Leitherer, C., & Schmitt, H. 2003, MNRAS, 339, 772
Rigopoulou, D., Kunze, D., Lutz, D., Genzel, R., & Moorwood, A. F. M. 2002, A&A, 389, 374
Rowan-Robinson, M., & Crawford, J. 1989, MNRAS, 238, 523
Rush, B., Malkan, M. A., & Edelson, R. A., 1996, ApJ, 473, 130
Rush, B., Malkan, M. A., Fink, H. H., & Voges, W. 1996, ApJ, 471, 190
Rush, B., Malkan, M. A., & Spinoglio, L. 1993, ApJS, 89, 1 (RMS)
Schmitt, H., Storchi-Bergmann, T., & Cid Fernandes, R. 1999, MNRAS, 303, 173
Spinoglio, L., Andreani, P., & Malkan, M. A. 2002, ApJ, 572, 105
Spinoglio, L., & Malkan, M. A. 1989, ApJ, 342, 83
_____. 1992, ApJ, 399, 504 (SM92)
Spinoglio, L., Malkan, M. A., Rush, B., Carrasco, L., & Recillas-Cruz, E. 1995, ApJ, 453, 616
Spinoglio, L., Malkan, M. A., Smith, H. A., Gonzalez-Alfonso, E., & Fischer, J. 2005, ApJ, 623, 123
Spinoglio L., et al. 2003, ASP Conf. Ser. 290, Active Galactic Nuclei: from Central Engine to Host Galaxy, ed. S. Collin, F. Combes & I. Shlosman (San Francisco: ASP), 557
Storchi-Bergmann, T., et al. 2001, ApJ, 559, 147
Swinyard, B., et al. 2008, Exp. Astron., 23, 193
Thean, A., et al. 2000, MNRAS, 314, 573
_____. 2001, MNRAS, 325, 737
Tommasin, S., Spinoglio, L., Malkan, M. A., Smith, H., Gonzalez-Alfonso, E., & Charmandaris, V. 2008, ApJ, 676, 836
Tran, H. D. 2001, ApJ, 554, L19
_____. 2003, ApJ, 583, 632